Energy materials

Epoxy-embedded silver nanowire meshes for transparent flexible electrodes

Lei Miao[1,2] , Guojun Liu[2,*] , Kevin McEleney[2] , and Jiandong Wang[2]

[1] Foshan University, 18 Jiangwan 1st Road, Foshan 528000, Guangdong, People's Republic of China
[2] Queen's University, 90 Bader Lane, Kingston, ON K7L 3N6, Canada

ABSTRACT

Spreading a Ag nanowire (NW) dispersion using a bar coater onto a poly(-ethylene terephthalate) (PET) film and evaporating the solvent yielded a transparent NW mesh. Further spreading a solution of bisphenol A diglycidyl ether and hardeners over this mesh using the bar coater and curing the epoxy precursors produced an epoxy-embedded NW mesh or an embedded NW electrode. Various techniques including scanning electron microscopy, transmission electron microscopy, and measurements of sheet resistance and transmittance were used to monitor the electrode fabrication process, which involved NW synthesis, casting NWs onto PET or glass substrates, subjecting the NW mesh to plasma treatment, and mesh embedment by an epoxy. Using our casting method, the areal density of the spread NWs and the thickness of the epoxy layer could be readily tuned by changing the concentrations of the NW dispersion and the epoxy precursory solution concentration, respectively. Our optimized electrodes had a Ag mass density of 1.0×10^{-5} g/cm^2 in the NW mesh, embedded in an epoxy layer with a thickness of 0.6 μm. While many of the NW junctions in the mesh were locked in the coating matrix, sections of the NWs were arched over the epoxy layer to provide the required electrical contact with external devices. The optimized electrodes had a sheet resistance R_s value of 18.9 ± 4.8 Ω/□ and a transmittance (T%) of $86.5 \pm 0.3\%$ at 550 nm. In addition, the embedded electrode withstood 500 cycles of bending, 500 repetitions of rubbing, and over 100 cycles of an adhesion tape test without noticeable deteriorations in their R_s and T% values. Furthermore, their high-temperature stability and sulfurization resistance were significantly enhanced over those of the unembedded electrodes and they also withstood soaking in ethanol and acetone. The ready availability and affordability of the epoxy formulation and the high control of the epoxy deposition protocol suggest that this electrode fabrication strategy has significant practical value.

Address correspondence to E-mail: guojun.liu@chem.queensu.ca

 Springer

Introduction

Transparent conductive electrodes are widely used in many applications [1]. For example, transparent electrodes allow touchscreen displays of tablets and cellphones to respond to the stroke of a fingertip. As one electrode of a solar cell or a light emitting device, it allows light to enter or leave the cell while simultaneously conducting electricity.

Today's transparent electrodes are mostly made from indium tin oxide (ITO). However, ITO electrodes have limitations. First, the costs of these electrodes are increasing mainly due to the gradual depletion of the rare element indium from the planet. Second, ITO films are brittle and thus are ill-suited for use in flexible devices. Thus, the development of alternatives for ITO has been a hot research topic in recent decades [1].

Among the various alternatives, including overlapping graphene sheets and carbon nanotube networks [1], silver nanowire (NW) meshes are very promising due to several considerations [2–5]. First, Ag is a better conductor than carbon-based graphene and nanotubes. Second, facile methods exist for the synthesis of NWs at high length-to-diameter aspect ratios [5, 6]. Third, long NWs can be readily cast to yield a percolating conductive mesh even at a very low NW areal density [7, 8]. While the crossing of each NW by many others reduces the contact resistances of the mesh, the use of NWs at a low areal density reduces materials cost and ensures a high light transmission through the mesh. Finally, a NW mesh welded by heat [2], pressure [3], light [9, 10], or plasma [11] is highly flexible and allows its use in bendable devices.

Despite the advantages of NW meshes as transparent electrodes, an uncoated NW electrode offers poor adhesion to a substrate and lacks abrasion resistance. Further, naked NWs show poor chemical resistance against oxidation and other undesired reactions. Thus, improving these properties would represent a critical step toward realizing applications of electrodes based on NWs. This paper reports the embedment of NW meshes in an epoxy formulation to yield robust electrodes that have much improved adhesion to their substrates, excellent abrasion resistance, and high chemical stability.

Indeed, there have been reports on the coating of NW meshes to yield more robust electrodes. For example, NW meshes have been overcoated with graphene or graphene oxide [12–15] layers to shield them from air and moisture, resulting in increased air stability of the electrodes. Other inorganic materials used to overcoat NW meshes have included ZnO [16] or Al_2O_3 [17] that were applied via chemical vapor deposition or sputter coating, or TiO_2 [18, 19], which was deposited via sol–gel chemistry. Examples of polymers used as the coating material have included a UV crosslinkable polyurethane [20], a photoresist [21], a UV curable epoxy [22], polydopamine [23], poly(dimethylsiloxane) [24], poly(vinyl alcohol) [25], and polycarbonate [26].

When polymers were used, the applied polymer layers were normally thicker than several micrometers [20, 22, 24] and such thick coatings led to the burial of the NW meshes within the coatings. While this full shielding by these thick coatings provided a greater degree of protection to the NWs, the burial also reduced the accessibility of the NW meshes for electrical contact. One way to address this issue has been to detach an overcoated electrode from the original substrate, thus exposing the NW mesh lying at the very bottom of an overcoated electrode [24, 25]. Another approach has been to etch the polymer off the edges of a buried NW mesh to re-establish electrical contact between the metal mesh and external devices [22].

In this study, we have chosen not to overcoat or bury NW meshes in a coating. Rather, we used an epoxy coating with a thickness of 0.6 μm to embed a NW mesh. An epoxy was used because it is affordable and has a high tensile strength, good thermal stability, and good chemical resistance [27, 28]. Epoxies also bind strongly to numerous substrates [29] and have been used commercially as binders for conductive adhesives [30, 31]. At the optimized thickness of ∼ 0.6 μm, the coating still provided the electrode with the desired substrate adhesion, rubbing resistance, and chemical stability. More importantly, the embedding did not prevent sections of the NWs from making electrical contacts with external devices. Thus, a robust electrode was directly obtained after an optimized amount of an epoxy formulation was cast to embed a NW mesh.

Experimental section

Materials

Silver nitrate ($AgNO_3$, ACS reagent grade), anhydrous ferric chloride ($FeCl_3$, 97%), ethylene glycol (EG, Reagent Plus, > 99.0%), poly(vinyl pyrrolidone) (PVP, $M_w = 1.30 \times 10^6$ g/mol), bisphenol A diglycidyl ether (DGEBA), poly(propylene glycol) bis(2-aminopropyl ether) (Jeffamine, $M_n \approx 230$ g/mol), piperazine (anhydrous, 99%), and triethanolamine (99%) were purchased from Sigma-Aldrich. Industrial grade ethyl alcohol (95 vol%) was acquired from Commercial Alcohol. All of the chemicals were used as received without further purification. PET films (8.5″ × 11″ in area and 0.0050″ in thickness, DuraLar™) were purchased from Grafix®, and each was cut into four pieces with dimension of 4.2″ × 5.5″ before use.

NW synthesis

NWs were synthesized using a modified literature method [32]. PVP (0.30 g, 27 mmol of VP units) was first dissolved in 50 mL of ethylene glycol in a round-bottom flask. The mixture was then stirred at 130 °C for 30 min to remove volatile impurities, which should have escaped through the loosely set glass stopper. The solution was then carefully sealed and cooled to room temperature. $AgNO_3$ (0.200 g, 1.20 mmol) and 10.0 μL of a $FeCl_3$ solution at 62.5 mmol/L in ethylene glycol were then added and mixed by magnetic stirring. The mixture was lastly transferred into a 100-mL Teflon hydrothermal reactor (Boshi Electronic Inc.), which consisted of an enclosed Teflon cylindrical cell in a thick-walled pressure-proof stainless-steel case. The reactor was subsequently placed in a preheated oven at 130 °C for 10 h to produce NWs. The Teflon cell served to reduce NW adsorption by the cell walls.

During subsequent purification, the crude product containing spherical particles and short NWs was diluted with 200 mL of acetone and centrifuged at 640 g_0 for 2 min. The supernatant was then decanted, and the precipitate was re-dispersed into 25 mL of ethanol. The resultant dispersion was diluted with another 200 mL of acetone before it was centrifuged at 1200 g_0 for 5 min. After supernatant decantation, the loose precipitate was dispersed in 10.0 mL of ethanol. The concentration of this dispersion was

determined from the solid residual after 1.00 mL of it had evaporated. This dispersion was further diluted with ethanol to 4.0 mg/mL for the preparation of NW networks.

NW meshes in epoxy on PET

A PET film, 4.2″ × 5.5″, was first treated for 15 min in a 100 W Harrick PDC-32G plasma cleaner with air pressure set at 600 millitorrs and its RF coil set at a direct current density of 15 mA, a voltage of 700 V, and a power of 10.5 W. Subsequently, 500 μL of the NW dispersion (in ethanol at 4.0 mg/mL) was dispensed onto the PET film before a Gardco® film coater that had a path gap of 25.4 μm and path width of 3″ was slowly drawn across the dispersion puddle to remove the superfluous liquid. This was followed by ethanol evaporation and plasma treatment for 3 min under the conditions described above.

To bind the NW network to the PET film, 600 μL of a DGEBA/hardener solution in ethanol at a concentration of 20, 40, or 67 mg/mL was dispensed on the network. The mixture was then spread on the NW-covered PET film using the film coater mentioned above. After solvent evaporation, the film was cured in an oven at 110 °C for 48 h.

The hardener consisted of Jeffamine, triethanolamine and piperazine at the mass ratios of 1.000/0.106/0.034. Using the active H number or reactive site numbers of 4, 3, and 2 for the three components of the hardener mixture, the used recipes represented a molar ratio of 1.00/1.00 between the epoxide rings in DGEBA and the active H atoms in the hardener mixture [33].

SEM analyses

Scanning electron microscopic (SEM) images were captured using a FEI 650-FEG instrument or a FEI Quanta 250 instrument that was operated in the environmental mode at an accelerating voltage of 10 kV. Both backscattered electron and secondary electron images were collected depending on the configuration of the instruments. Energy-dispersive X-ray spectroscopy using an EDAX Element detector was performed on the Quanta 250 instrument. To prepare a NW specimen, a drop of a NW dispersion in ethanol (~ 0.10 mg/mL) was dispensed onto a silicon wafer (0.5×0.5 cm^2) and the solvent was evaporated under ambient conditions. To obtain a

top-down view of a NW mesh embedded in the epoxy, a small piece (0.5×0.5 cm^2) was cut from such an electrode using a surgical knife and the thus obtained sample was then pressed with the PET side facing downward onto a double-sided conductive tape that had already been placed on a stainless-steel stub (sample holder). To obtain a cross-sectional view, a PET substrate bearing NWs was cut into pieces from the NW-bearing side by a sharp surgical knife and then was glued using a double-sided adhesive tape onto a side of a stainless-steel stub.

Other analyses

Atomic force microscopy (AFM) images were obtained using a Nanoscope IIIA (Veeco) instrument that was operated in the tapping mode. The transmittance values $T\%$ of the electrodes at 550 nm were measured with a Cary 300 Bio (Varian) spectrometer, and an uncoated PET film was used as the reference. The surface resistance (R_s) of the sample was measured in at least 10 regions for each sample using a RM3000 Plus test unit (Jandel). The contact diameter of each probe was 500 μm, and the spacing between two neighboring probes was 0.50 mm. The current that was applied to the probes was fixed at 10 μA.

Transmission electron microscopy (TEM) was performed on a Thermo Fisher Talos L120C at an accelerating voltage of 120 kV equipped with a 16-megapixel CETA camera for image acquisition. The instrument was also configured for scanning transmission electron microscopy (STEM) with a high-angle annular dark-field (HAADF) detector. Samples for TEM were prepared by dispersing a drop of the ethanol-based NW dispersion on a Cu grid, allowing the solvent to evaporate at room temperature, leaving a residual film of NW on the grid.

Thermal stability

The electrodes used for this test were prepared on glass slides. The cured electrodes were then placed into a KSL-1100X muffle furnace (MTI Corp.) and baked in air at different temperatures. At an interval of 5 or 10 min, the samples were taken out and cooled to room temperature to measure their surface resistance R_s.

Bending tests

Prior to this test, the samples were cut into rectangular strips with dimensions of 5.0×1.0 cm^2. The middle section of a strip with the electrode-bearing side facing outwardly was then bent into a semicircle with a diameter of 1.0 cm. This was followed by the release of the force and the restoration of the strip's original shape. The R_s values were measured for samples in the bent sections after they had been subjected to pre-designated numbers of cycles.

Wear tests

The samples were cut into circles with a diameter of 8.5 mm and then glued onto the bottom of a 100 g weight using double-sided adhesive tape. Each wear test involved pushing this weight using a horizontal force forward or backward for 10 cm on a piece of cotton fabric. The R_s and $T\%$ values were recorded for the samples after they were subject to pre-designated numbers of this wear test.

Adhesion test

A piece of a Scotch® transparent tape with dimensions of 1.9×1.9 cm^2 was pressed onto an electrode using a force of ~ 10 N. The tape was then removed by hand.

Scratch tests

A sharpened 2B pencil was mounted into a 501 pencil hardness tester (Elcometer Inc.). The tester was then placed on an electrode and pushed forward horizontally. The scratch left behind on each electrode was then observed via SEM.

Chemical resistance tests

The samples were immersed into acetone or ethanol for pre-designated durations and then removed. After the solvents were evaporated in an oven at 80 °C and cooled to room temperature, their R_s and $T\%$ values were recorded.

Sulfurization test

The samples were immersed in a 0.20 mg/mL sulfur solution for 30 min. After rinsing the soaked samples by ethanol and drying in an oven at 80 °C, their R_s

and $T\%$ values were recorded after cooling to room temperature.

Results and discussion

NW synthesis and characterization

The NWs were synthesized via the reduction of AgNO$_3$ by ethylene glycol, which also served as the solvent, using poly(vinyl pyrrolidone) (PVP) as the dispersant [32]. To increase the length of the NWs, AgCl crystals that formed at room temperature were used as the seeds for Ag growth [34, 35]. The crude product in ethylene glycol was then diluted with acetone, a poor solvent for PVP, and centrifuged at a low centrifugal force of 640 g_0 to settle and separate the longer NWs from the Ag nanospheres, short NWs as well as residual PVP that remained in the supernatant. After the pellet containing the NWs was re-dispersed in ethanol, this dispersion was diluted with acetone again prior to the repetition of the centrifugal fractionation step. The final NW precipitate was re-dispersed into ethanol, and its concentration was adjusted to 4.0 mg/mL for future use.

Figure 1a, b shows SEM images of the fractionated NWs after they had been cast onto a silicon wafer from ethanol. The sample was essentially free of spherical particles. Analysis of 30 NWs yielded an average length and diameter of 34 ± 6 μm and 129 ± 23 nm, respectively, and these values suggest that the NWs had relatively narrow length and diameter distributions. TEM characterization of the NWs (Fig. 1c) confirms the NW structure while showing the uneven polymer coating covering the wires.

This rugged PVP layer observed by TEM was not consistent with the uniform PVP coating observed before [6]. The TEM specimens were prepared by evaporating a drop of an NW suspension on a copper grid. If free PVP was present in ethanol, the evaporation of this solvent would have left PVP on the NWs. Thus, the rugged layer was probably formed during TEM specimen preparation.

If free PVP existed in the ethanol phase, its concentration was likely low. We performed a thermogravimetric analysis (TGA) of the NWs and a weight loss of merely 3.1% was observed when the NWs were heated under a nitrogen flow from 120 to 800 °C, by which point Ag should remain and PVP should have lost most of its weight except the carbonized fraction. Because of this carbonization, the actual PVP content could exceed 3.1 wt%. However, a prior comparative thermogravimetric study of PVP decomposition under both nitrogen and air suggested that the carbonized fraction of PVP under N$_2$ should be less than 50% [36].

Because only a small amount of free PVP was present, we did not remove the free PVP from the NWs. Further, the PVP layer would be removed later by subjecting the NW networks to plasma treatment before they were embedded into the epoxy.

PVP removal and NW welding by plasma

The PVP layer on the surfaces of the NWs was detrimental in two ways. First, PVP has a low bulk conductivity [37] of 6.6×10^{-8} S/m and its presence should increase the contact resistance between different NWs, thus imparting the resultant mesh with a high sheet resistance. Second, PVP does not contain groups that bind with functionalities of most epoxy formulations and its presence should weaken the
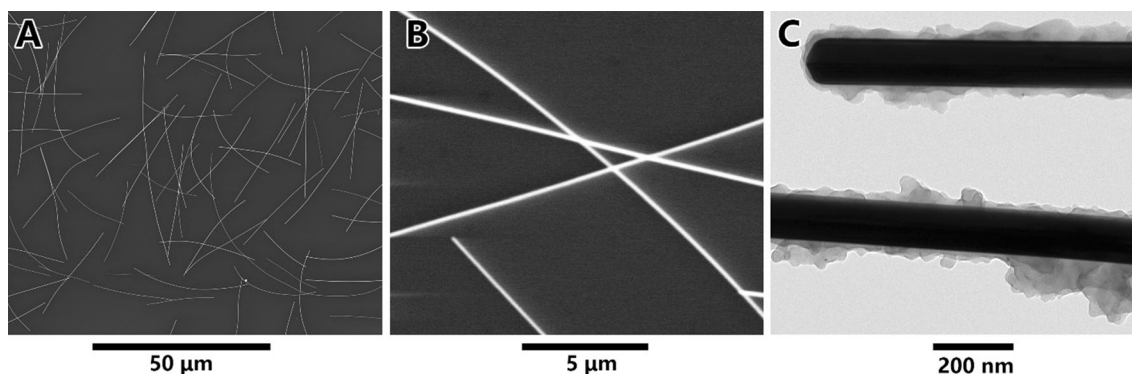
Figure 1 **a** and **b** Backscattered SEM images of NWs on a silicon wafer and **c** a TEM image of NWs suspended on a Cu grid.

binding between the NWs and an epoxy, yielding a compromised electrode. We did not remove PVP using dramatic measures such as treating the wires with NaBH₄ [38] before the deposition of the NWs because naked NWs would not remain dispersed in solvent.

We removed the PVP by subjecting NWs to an air plasma for 3 min under conditions detailed in the "Experimental" section. Figure 2a shows a TEM bright field image of NWs after the plasma treatment, and little of the polymer layer observed in Fig. 1c remains on the NWs. Thus, the plasma treatment successfully removed most of the PVP layer.

Interestingly, some new dark spherical nanoparticles are seen in Fig. 2a. To gain insight into the composition of these particles, scanning transmission electron microscopy (STEM) was used to study the sample. Figure 2b shows a high-angle annular dark-field (HAADF) image of some NWs. Comparing the contrast of the spherical nanoparticles to the NWs suggests that they are similar in composition. Thus, the particles are likely Ag nanoparticles or Ag nanoparticles that were partially oxidized in the air plasma.

The removal of PVP by plasma and the formation of Ag nanoparticles from NWs under plasma treatment should not be surprising. Plasma has been used previously to etch PVP from NWs [11, 39] and has been used to chemically modify many surfaces [40]. The Ag nanoparticles were formed via the local melting of the NWs after they were bombarded by electrons and ions during plasma treatment. Other researchers have shown that NWs could melt, weld, fragment, and become fused under prolonged plasma treatment [11]. We did not prolong the plasma treatment beyond 3.0 min to avoid NW fragmentation, which would degrade conductivity. We believe that the plasma treatment not only removed PVP but also helped with welding the NWs.
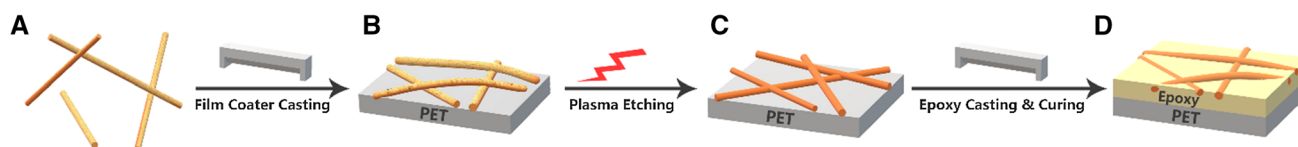
Electrodes

Electrodes were applied onto PET substrates via the following steps. First, the PET substrate was treated with air plasma to generate some polar functionalities, which increased the wettability of the PET surface by polar solvents such as ethanol and water [41, 42]. Second, a controlled amount of NWs was cast onto the treated PET (A → B, Scheme 1). Third, the cast NW mesh was treated by plasma again to remove PVP and to partially weld the NWs (B → C). Lastly, a controlled amount of an epoxy precursor mixture was cast, spread, and cured to "lock" the NW mesh in position and to thus bind the mesh to the PET substrate.

The areal density of NWs, corresponding to the number or mass of NWs cast per unit PET surface, was a critical factor influencing the quality of an electrode. As the NW areal density increased, the sheet resistance R_s and the light transmittance $T\%$ of a NW mesh decreased [4]. We prepared NW meshes by dispensing a NW dispersion onto a plasma-treated PET substrate and then spreading the dispersion by drawing a bar coater that possessed a gating height of 25.4 μm across the dispersion puddle, leaving behind a dispersion film with a thickness of 25.4 μm. Evaporating the solvent ethanol subsequently yielded a NW mesh. Since the volume of the

Figure 2 **a** TEM and **b** STEM HAADF images of NWs on a TEM grid after plasma treatment.

200 nm

200 nm
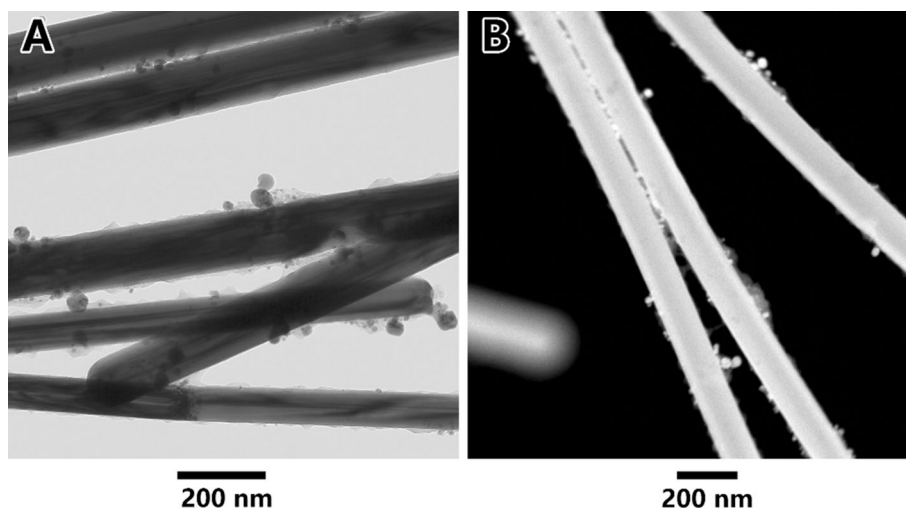
Scheme 1 Process for fabricating an epoxy-embedded electrode. **A → B**: NW casting onto PET by a film coater; **B → C**: PVP layer removal from NW surfaces by plasma; **C → D**: NW embedment by the epoxy.

dispersion film left behind per cm^2 immediately after a bar coater was drawn across should be 2.54×10^{-3} cm^3, we regulated the cast NW amount per cm^2 by adjusting the concentration of the NWs in ethanol. Our systematic study eventually revealed that the best compromise between R_s and $T\%$ was achieved when the meshes were prepared using an NW dispersion concentration of 4.0 mg/mL. At this concentration, the areal mass density of the NW mesh was 1.02×10^{-5} g/cm^2.

Figure 3a provides a top-down SEM image of such a NW mesh after it had been subjected to plasma treatment. In the mesh, each NW possessed more than one junction with other NWs. Despite mesh formation, the number of NW layers did not exceed three and the areal density of NWs was low. The dark grooves observed beneath those sections of the NWs that were in contact with the PET provided evidence of the plasma treatment. These grooves were formed probably due to the thermal decomposition of PET adjacent to the heated NW sections during plasma treatment. Moreover, the NWs could be imaged with sharp contrast as seen in Fig. 3a despite the use of a secondary electron detector. Secondary electrons are known to have shallow penetration depths into most materials [43], and that they could be used to form the image rendered support for the removal of the PVP surface layer by plasma.
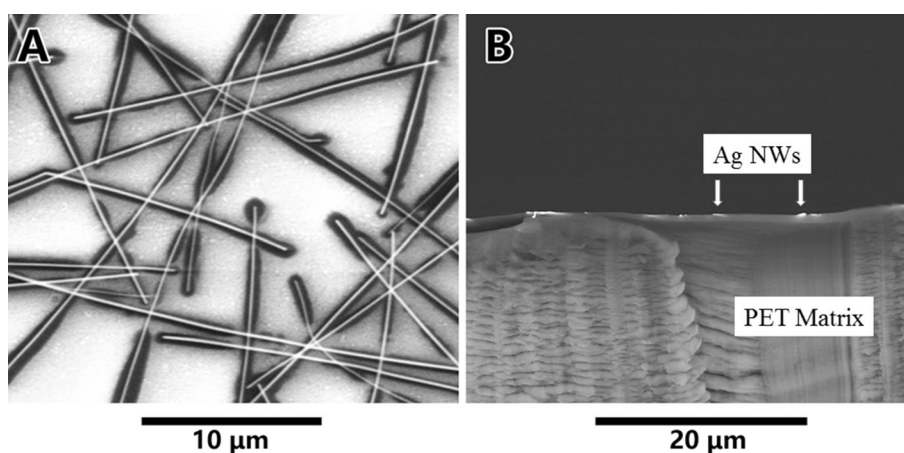
Figure 3b shows a cross-sectional view of such a mesh after the sample on PET was cut with a surgical knife. Sections of the different NWs were seen only at certain spots as would be expected for the cross section of a mesh. The PET matrix appeared wrinkled probably due to deformation during sample cutting. The high contrast between the NWs and the matrix was again due to the removal of PVP by plasma from the NW surfaces.

The NW meshes prepared under our optimized conditions had an R_s value of 18.2 ± 3.5 $\Omega/\square$ prior to plasma treatment. After plasma treatment, the R_s value was reduced to 12.1 ± 2.0 $\Omega/\square$. This R_s reduction was predicted as the plasma treatment removed PVP and possibly also facilitated the welding of some NW junctions [11].

A highly transparent epoxy formulation that we have used previously [33] was utilized in this study to lock in the NW mesh structure and to bind it to the PET substrate. As mentioned in the "Experimental" section, the formulation used bisphenol A diglycidyl ether as the epoxy resin and a mixture of three hardeners for the resin. The mixture was applied onto NW meshes at the resin/hardener concentrations of 20, 40, or 67 mg/mL in ethanol with the use of the bar coater. Since the final coating solution film thickness was 25.4 μm, the thicknesses of the final coatings in the three cases were calculated to be 0.5,

Figure 3 a Top-down and **b** cross-sectional secondary electron SEM images of NWs after they were cast onto a PET film and then treated with plasma.

1.0, and 1.7 µm, respectively, by assuming a density of ~ 1.0 g/cm^3 for the final epoxy coating.

Figure 4a shows a cross-sectional backscattered electron SEM image of a NW electrode that had an epoxy layer thickness of 0.5 µm. Aside from one NW segment (pinpointed by a hollow arrow) that appeared embedded in the epoxy matrix, the others appeared to "float" on the surface of the binder. The two segments marked by solid arrows seemed bent and exposed probably because of the detachment of the NW segments from the binder during specimen cutting.

The "floating" of segments of the NWs to the surface of the epoxy binder is more evident in Fig. 4b, which shows the top-down backscattered SEM image of an NW electrode possessing an epoxy layer thickness of 1.7 µm. Despite the thickness of this epoxy layer, many NW segments were on the surface of the binder.

We have two plausible reasons for the "floating" of the NW segments on the epoxy surface. First, the epoxy layer probably got cured starting from the bottom due to heat transfer through the substrate. The movement of the curing front pushed the NWs up during the epoxy crosslinking process. Second, the NWs arched over the coating. The arches could also have formed during the epoxy curing process, which could not have occurred simultaneously and uniformly throughout a coating and the faster curing in certain regions could have forced the NWs to arch somewhat.

Evidence for the arching of the NWs could be gleaned from examining Fig. 4b more closely. While each NW appeared essentially uniformly bright in Fig. 1b due to the efficient backscattering of the electrons by the NWs, many of their counterparts in Fig. 4b contained dark sections, as indicated by the arrows. In addition, the dark sections appeared more frequently at the "end" of a NW before it disappeared from view. A plausible explanation for the dark sections in Fig. 4b was that these regions were more heavily coated by epoxy. The backscattered electrons used for the formation of Fig. 4b had a penetration depth of ~ 100 nm through the coating layer [43]. Thus, they could be detected from NWs only in sections that bore a coating that was thinner than ~ 100 nm and the sections that were more heavily coated appeared dark. The density of the dark sections near the "ends" of some NWs increased probably because the NWs arched over the PET film and these "ends" were not the actual physical termini but appeared as "ends" because they entered the epoxy film.

Despite the "floating" and arching of the NWs, we suspect that the top surface of the NWs should be somewhat coated. The facile coating of Ag by epoxy should be easy to understand because the surface energies of Ag[100] [44] and DGEBA [45] are 1.2×10^3 and 38.8 mJ/m^2, respectively, and the spreading of a low-surface-energy liquid on a high-surface-energy substrate should be favorable according to Young's equation [46]. While the coating provided the desired protection for the NWs as will be discussed subsequently, its thinness ensured that the electrons were able to tunnel through it under a suitable bias voltage for device applications [47].

The thinness of the epoxy coating was supported by the fact that the embedding of the NWs in the epoxy coatings did not significantly increase the sheet resistance of the final electrodes from the initial value

Figure 4 **a** Cross-sectional and **b** top-down backscattered electron SEM images of a NW/epoxy film on a PET plate.
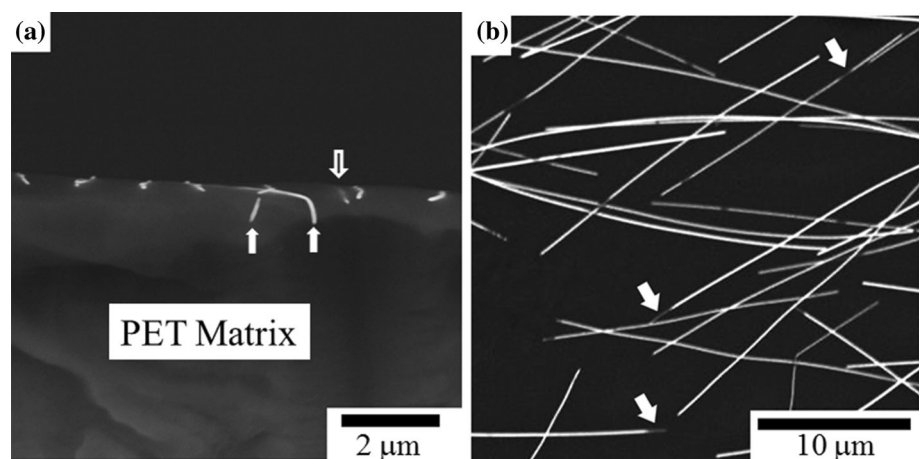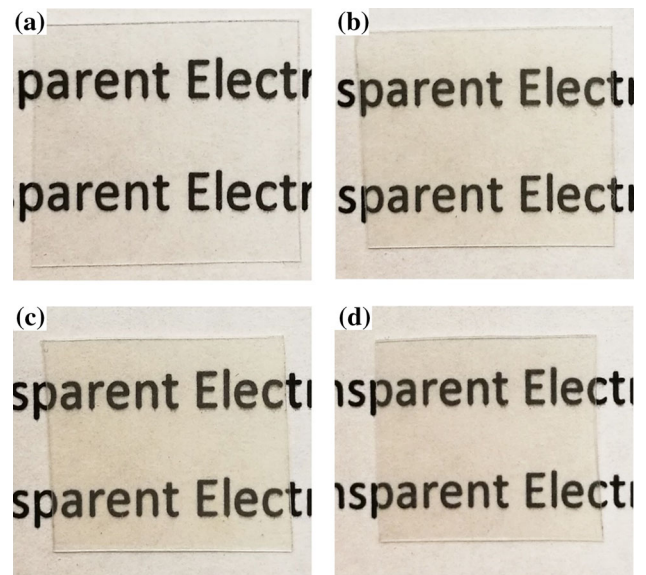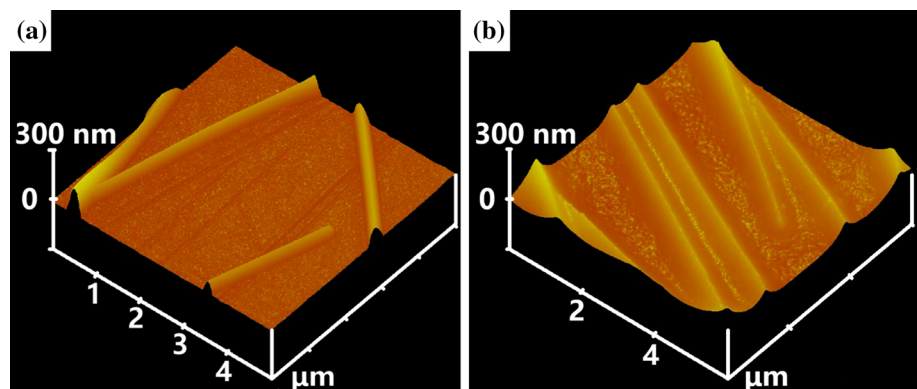
of 12.1 ± 2.0 $\Omega/\square$ for the bare electrode. The R_s values of the meshes embedded in epoxy coatings with thicknesses of 0.5, 1.0, and 1.7 μm were 18.9 ± 4.8, 21.6 ± 6.6, and 22.8 ± 7.4 $\Omega/\square$, respectively.

AFM was also used to study the electrodes before and after the application of an epoxy layer of the thickness of 1.0 μm (Fig. 5a, b). While the coated NWs had an average diameter of 388 ± 52 nm, that for the uncoated ones was 172 ± 13 nm. The much larger average diameter of the NWs was due to the fact that the "floating" wires were partially immersed in the coating.

Transparency

The optical transparency of the embedded electrodes on PET with epoxy thicknesses of 0.5, 1.0, and 1.7 μm was assessed. Figure 6 compares photographs of a PET film alone and the three PET films covered by embedded electrodes that were placed above a piece of paper marked with the repeated phrase "Transparent Electrode." The words behind the electrodes were clearly legible in each case. Quantitatively, the transmittance values $T\%$ for the three electrodes at 550 nm were $86.5 \pm 0.3\%$, $86.8 \pm 0.3\%$, and $87.5 \pm 0.5\%$, respectively, as the thickness of the epoxy film increased. $T\%$ barely changed with the epoxy film thickness because the epoxy coating did not absorb light at 550 nm and a 30-μm-thick epoxy coating had a transmission higher than 99.5% [33]. In fact, one can plausibly argue that $T\%$ decreased as the epoxy coating thickness increased probably due to the replacement of the low-refractive index air in the inter-wire space with the higher refractive index epoxy, resulting in reduced light scattering. Thus, the electrodes were promising candidates for display applications.
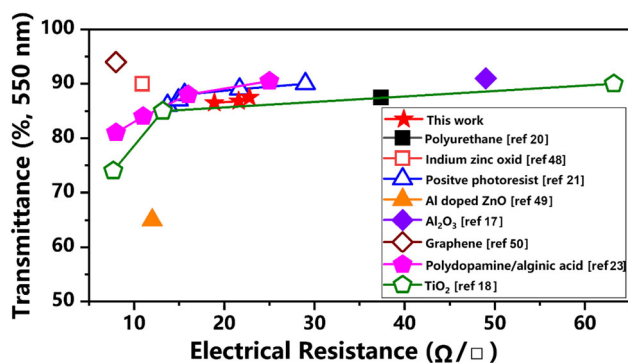
Figure 6 Photographs of **a** a PET film and PET films bearing embedded NW electrodes at the epoxy thickness of **b** 0.6, **c** 1.2, and **d** 1.7 μm, respectively. The samples were placed on paper marked with the repeated phrase "Transparent Electrode".

Comparison with other NW electrodes

Our electrode at an epoxy coating thickness of 0.6 μm had the R_s and $T\%$ values of 18.9 ± 4.8 $\Omega/\square$ and $86.5 \pm 0.3\%$, respectively. These values match those obtained with the top-end ITO electrodes currently available on the market [4], thus demonstrating the potential of our NW electrodes for practical applications.

As mentioned in Introduction, various polymers and inorganic materials have been used to coat NW meshes to enhance their robustness. Figure 7 plots the $T\%$ values of our electrodes as a function of their R_s values and those of NW electrodes coated by other materials. Our data are comparable with or exceed

Figure 5 3D AFM images of NWs on a PET substrate **a** before and **b** after embedding in an epoxy coating with a thickness of 1.2 μm.

Figure 7 Plots of transmittance values of NW electrodes prepared using various binding agents including polyurethane [20], indium zinc oxide [48], positive photoresist [21], Al-doped ZnO [49], Al_2O_3 [17], TiO_2 [18], polydopamine/alginic acid [23], and graphene [12].

those of other electrodes, except those coated by graphene. The electrodes coated by graphene had exceptionally high conductivity because graphene itself was conductive. However, no data were reported on the binding strength of NW electrodes that were overcoated by a monolayer of graphene to different substrates or the scratch resistance of those electrodes.

Thermal stability

For display applications, a thin luminescent layer may need to be applied onto an electrode via a chemical vapor deposition (CVD) process at a high temperature [50]. Thus, the stability of the electrodes at temperatures higher than room temperature is an important consideration. The conductivity of NWs should decrease due to the oxidation of silver into silver oxide, which is an insulator. We demonstrated the advantageous heat stability of the embedded NW electrodes by monitoring changes in the R_s and $T\%$ values of the NW electrodes and the embedded electrodes at an epoxy thickness of 0.6 μm after they were baked at different temperatures for various times. The data reported below were all gathered for this type of embedded electrode because they exhibited the lowest R_s values. Figure 8 shows how the ratio R_s/R_{s0} between the resistances of the electrodes observed after and before thermal treatment changed with their baking time in an air-saturated oven at 200, 250, 300, or 350 °C.

The data shown in Fig. 8 reveal that the two types of electrodes were stable during the observation

period of 55 min at 200 and 250 °C. At 300 °C, the R_s value for the unembedded electrode exceeded the upper detection limit of our instrument ($\sim$ 2.0 kΩ/ $\square$) between 5 and 10 min. To facilitate visual inspection of this trend, we arbitrarily assigned an R_s/ R_{s0} value of 100 at 10 min of baking time for this sample and the R_s/R_{s0} values at different heating times at this temperature are connected by a spline curve in Fig. 8a. At 300 °C, the R_s value of this electrode shot up to an unmeasurable value sometime between 0 and 5 min and the R_s/R_{s0} value at 5 min was arbitrarily assigned a value of 100 to enable to draw the spline curve. Figure 8b shows the data observed for the embedded electrodes. At 300 °C, a finite R_s/R_{s0} value of 11 ± 7 was measured after it was heated for 55 min. The R_s/R_{s0} value of such an electrode did not increase at all after heating at 350 °C for 5 min. Therefore, the embedded electrodes were more stable at elevated temperatures than the uncoated ones.

The enhanced thermal stability of epoxy-coated NWs was anticipated because the DGEBA-based epoxy resin is stable up to 300 °C and decomposes over the temperature range of 300–450 °C [51]. In the presence of an epoxy coating layer, oxygen needed to diffuse through this layer to react with Ag, which should inhibit the oxidation process.

Abrasion and adhesion tests

Embedding a NW network into a PET-binding epoxy layer should increase the abrasion resistance of the network and enhance its adhesion to the substrate. For the abrasion resistance tests, we glued an electrode to the bottom of a weight that exerted a pressure of 4.3 kPa on the electrode and rubbed the conductive side of the electrode against a swatch of cotton fabric. During each abrasion test, the weight was pushed either forward or backward by 10 cm each way. After rubbing an uncoated NW network on PET once, the NW layer was seen by the naked eye to be removed and its sheet resistance increased to values that exceeded our instrument's detection limit. Figure 9a shows how the R_s and $T\%$ (transmittance at 550 nm) values of the embedded electrode changed with the number of abrasion tests. After the embedded electrode had been subjected to 1000 cycles of the rubbing test, the R_s value increased from 18.8 ± 2.4 to 23.8 ± 7.2 Ω/$\square$ and the $T\%$ value remained essentially constant at 87%. Thus, the embedded electrode

Figure 8 Variations in the surface resistance R_s of NW electrodes that were **a** uncoated and **b** embedded in 0.6-μm-thick epoxy on glass plates as a function of electrode baking time at 200, 250, 300, and 350 °C, respectively.
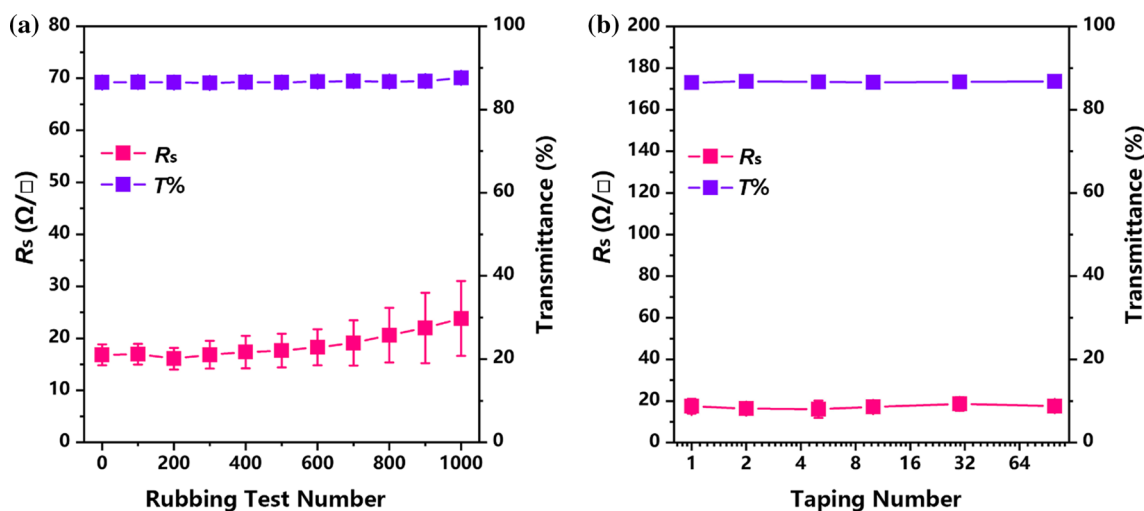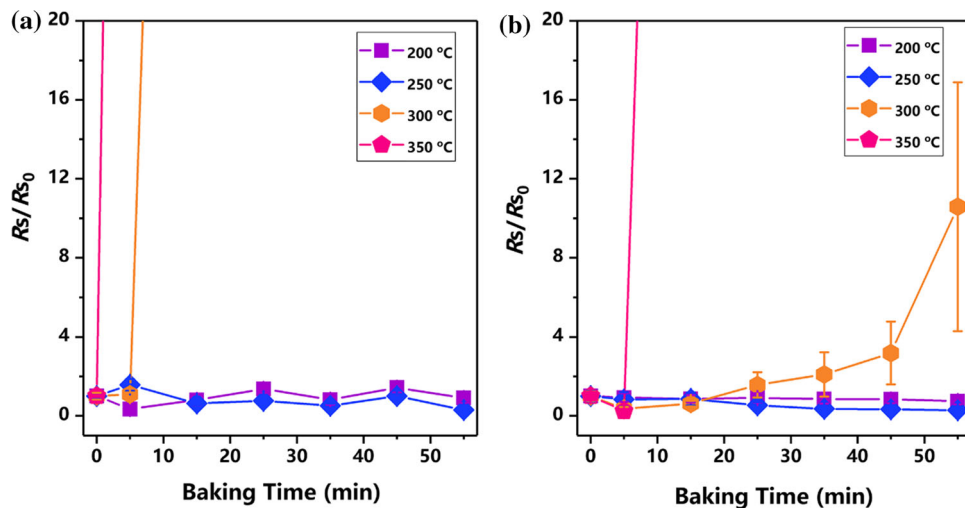
Figure 9 Plot of variation in the R_s and $T\%$ values of epoxy-embedded electrodes as a function of their number of repeated **a** rubbing and **b** taping tests.

was far more wear resistant than the unembedded electrode.

A tape test was used to evaluate the adhesion of the NW networks onto PET. In such a test, an adhesive tape was pressed onto an electrode and then pulled off. Without an epoxy coating, the NW network was seen to transfer onto the adhesive tape after only one test. In contrast, the embedded electrode remained on the PET substrate even after 100 repeated cycles of the tape test. Figure 9b shows how R_s and $T\%$ changed with the number of tape tests that an embedded electrode endured. R_s and $T\%$ remained essentially constant at $\sim$ 18.0 $\Omega/\square$ and 87% regardless of the number of tape tests. Thus, the embedded electrode possessed vastly superior adhesion to the PET substrate than was exhibited by

the unembedded electrode. This difference should not be surprising because epoxy is known to bind strongly to many substrates [29].

Bending test

A major advantage of a NW-based electrode is its flexibility or bendability [1]. To assess this property, we bent the middle section of an electrode on PET with the electrode-bearing side facing outwardly to a semicircle with a diameter of 1.0 cm and then released the ends to allow the electrode to recover its original shape, thus completing a bending cycle. After a pre-designated number of bending cycles, the R_s values of the electrode in the bent sections were measured. Figure 10 shows how the ratio R_s/R_{s0}
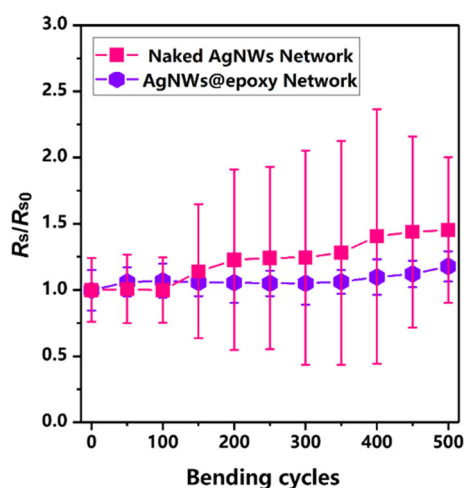
changed with the number of bending cycles for electrodes that were embedded and not embedded in the epoxy, respectively.

Figure 10 shows that the average R_s/R_{s0} value increased by 41% and the spread in the measured R_s values increased after the epoxy-free electrode withstood 500 bending cycles. While these results are superior already in comparison with ITO electrodes [52], the embedded electrode exhibited even more impressive properties. Their R_s/R_{s0} value remained essentially constant after 500 bending cycles and the variation in the measured R_s values remained low. This enhanced stability of the embedded electrode could be due to the reduced likelihood for the different NWs locked in an epoxy to detach from each other and to disrupt electrical contact during each electrode bending.
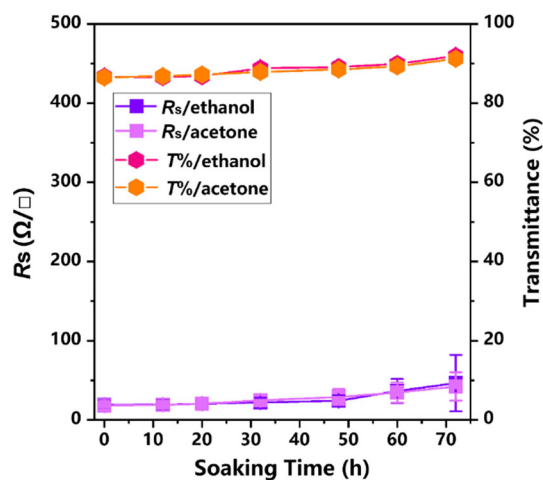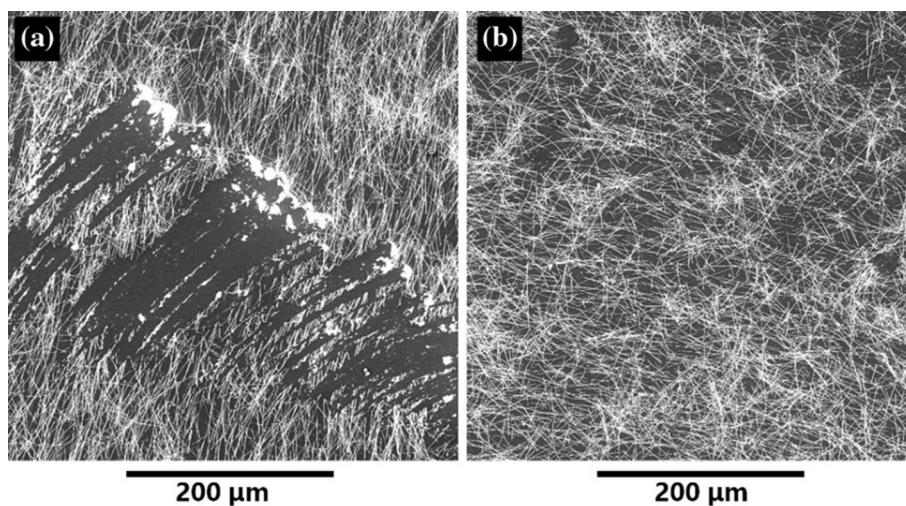
Scratch resistance

The bare and embedded NW electrodes were scratched with a pencil that had a hardness rating of 2B. Figure 11a shows an SEM image of a trace left behind by a pencil stroke on an unembedded electrode. While the mesh was severely damaged in this case, no such traces were visible in the SEM image of the embedded electrode after a similar test (Fig. 11b). Thus, the NWs were tightly bound to the epoxy matrix as predicted. The coating matrix was not
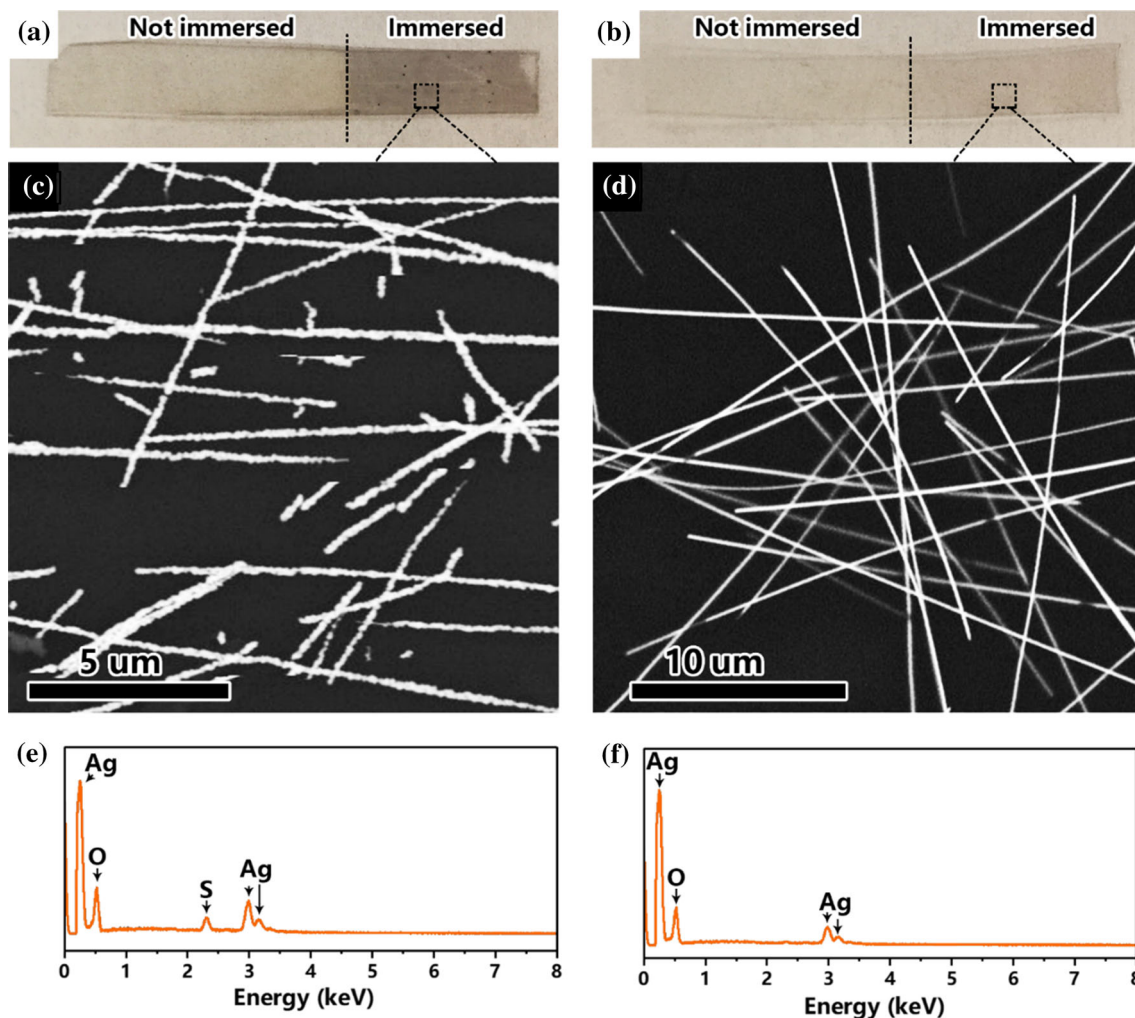
Figure 10 Variation in the R_s/R_{s0} values of bare and embedded electrodes as a function of the number of bending cycles.

Figure 12 Variation in the R_s and $T\%$ values of the epoxy-embedded electrodes as a function of their soaking time in ethanol or acetone.

Figure 11 SEM images of **a** a bare and **b** an embedded electrode after scratching with a pencil.

Figure 13 Photographs of two NW electrodes that were **a** bare and **b** embedded in epoxy after their bottom halves were immersed in a 0.20 mg/mL sulfur solution in ethanol for 30 min. Frames **c** and **d** show SEM images and frames **e** and **f** display the EDS spectra of the tarnished regions of the electrodes.

damaged by the pencil because the cured epoxy resin had a hardness of HB [53], which was harder than the pencil.

Chemical resistance

When used in a display device, an electrode may require cleaning with ethanol or acetone to remove smudge. Thus, such electrodes should be resistant against these solvents. We tested the solvent resistance of the bare and embedded NW electrodes by soaking them in ethanol or acetone and then drying them before performing R_s measurements. The R_s values of the bare electrodes increased to the detection limit of 2.0 kΩ/□ in many regions after they had been soaked in either ethanol or acetone for only 6 h

probably due to the spontaneous detachment of NWs from the PET substrate due to NW redispersion. In contrast, the R_s and $T\%$ values of the embedded electrodes remained constant after they were soaked in either ethanol or acetone for 30 h (Fig. 12) and increased only slightly between the soaking times of 30 and 70 h. Thus, the embedded electrodes were much more resistant to solvent soaking as predicted.

The electrodes were also subjected to a much tougher chemical resistance test. At room temperature, silver would react with sulfur to produce silver sulfide—a silver tarnish [54]. Figure 13a, b shows photographs of two electrodes after their bottom halves were immersed in a 0.20 mg/mL sulfur solution for 30 min. The immersed half of the unembedded electrode appeared dark or tarnished. On the

other hand, the immersed half of the embedded electrode was only slightly darkened, suggesting a reduced extent of Ag_2S formation in this case.

Figure 13c, d compares backscattered SEM images of the soaked regions of the bare and embedded electrodes after the sulfur soaking test. The NWs of the unembedded electrode appeared rugged due to Ag etching. In contrast, the NWs of the embedded electrode retained their smooth appearance.

The reaction of Ag with sulfur in the case of an unembedded electrode was unambiguously verified by the detection of a sulfur peak in the energy dispersion spectrum (EDS) of the rugged NWs, as shown in Fig. 13e. Meanwhile, the sulfur signal at 2.3 kV was barely noticeable in Fig. 13f for the embedded electrode. Thus, the results shown in Fig. 13 suggest that the embedded electrode exhibited sulfur resistance. The fact that even the sections of the NWs that arched over the epoxy film were resistant to tarnishing confirmed that these sections bore a layer of epoxy as we concluded based on the SEM and AFM images.

Conclusions

Silver nanowires were synthesized and then purified via centrifugal fractional precipitation. The resultant NWs had a length and diameter of 34 ± 6 μm and 129 ± 23 nm, respectively. Spraying a dispersion of the NWs at 4.0 mg/mL using a bar coater with a gapping height of 25.4 μm onto a PET substrate and subsequently evaporating the solvent yielded meshes that had a Ag areal density of 1.0×10^{-5} g/cm^2. In such a mesh, the NWs had random orientations and each wire was crossed by others multiple times. Treating the meshes for 3.0 min with an air plasma was shown by TEM to remove the poly(vinyl pyrrolidone) surfactant from the NWs and to decrease their sheet resistance.

The bar coater was also used to spread solution mixtures of bisphenol A diglycidyl ether and hardeners on the pre-deposited NW meshes. After solvent evaporation and thermal curing, NW electrodes embedded in epoxy were produced. The thickness of the epoxy coating could be readily tuned by varying the concentration of the epoxy precursor coating solution. At an epoxy thickness of 0.5 μm, the electrodes had a transmittance of $86.5 \pm 0.3\%$ at 550 nm and a sheet resistance of 18.9 ± 4.8 Ω/□. More

importantly, the embedded electrodes displayed vastly superior properties than their bare NW mesh counterparts. Unlike the naked NW meshes, the embedded electrodes were resistant to fabric abrasion and pencil scratching, strongly adherent to PET, resistant to tarnishing by sulfur, and readily withstood soaking in ethanol and acetone. Additionally, the epoxy coating improved the electrodes' high-temperature stability and resistance to bending. The embedded electrodes retained their original sheet resistance after they had been subjected to 500 cycles of a bending test, which involved bending an electrode into a semicircle with a diameter of 1.0 cm and allowing it to recover its original shape. Since the epoxy formulation is commercially available and readily affordable and the coating protocol is straightforward, the fabricated electrodes are promising candidates for practical applications.

Acknowledgements

References

[1] Hecht DS, Hu LB, Irvin G (2011) Emerging transparent electrodes based on thin films of carbon nanotubes, graphene, and metallic nanostructures. Adv Mater 23:1482–1513

[2] Lee JY, Connor ST, Cui Y, Peumans P (2008) Solution-processed metal nanowire mesh transparent electrodes. Nano Lett 8:689–692

[3] Hu LB, Kim HS, Lee JY, Peumans P, Cui Y (2010) Scalable coating and properties of transparent, flexible, silver nanowire electrodes. ACS Nano 4:2955–2963

[4] Langley D, Giusti G, Mayousse C, Celle C, Bellet D, Simonato J-P (2013) Flexible transparent conductive materials based on silver nanowire networks: a review. Nanotechnology 24:452001

[5] Zhang P, Wyman I, Hu JW, Lin SD, Zhong ZW, Tu YY, Huang ZZ, Wei YL (2017) Silver nanowires: synthesis

technologies, growth mechanism and multifunctional applications. Mater Sci Eng B-Adv 223:1–23

[6] Sun YG, Gates B, Mayers B, Xia YN (2002) Crystalline silver nanowires by soft solution processing. Nano Lett 2:165–168

[7] Seager CH, Pike GE (1974) Percolation and conductivity—a computer study ii. Phys Rev B 10:1435–1446

[8] Wu H, Hu LB, Rowell MW, Kong DS, Cha JJ, McDonough JR, Zhu J, Yang YA, McGehee MD, Cui Y (2010) Electro-spun metal nanofiber webs as high-performance transparent electrode. Nano Lett 10:4242–4248

[9] Garnett EC, Cai WS, Cha JJ, Mahmood F, Connor ST, Christoforo MG, Cui Y, McGehee MD, Brongersma ML (2012) Self-limited plasmonic welding of silver nanowire junctions. Nat Mater 11:241–249

[10] Chung WH, Kim SH, Kim HS (2016) Welding of silver nanowire networks via flash white light and UV-C irradiation for highly conductive and reliable transparent electrodes. Sci Rep 6:32086

[11] Li J, Tao Y, Chen SF, Li HY, Chen P, Wei MZ, Wang H, Li K, Mazzeo M, Duan Y (2017) A flexible plasma-treated silver-nanowire electrode for organic light-emitting devices. Sci Rep 7:16468

[12] Deng B, Hsu PC, Chen GC, Chandrashekar BN, Liao L, Ayitimuda Z, Wu JX, Guo YF, Lin L, Zhou Y, Aisijiang M, Xie Q, Cui Y, Liu ZF, Peng HL (2015) Roll-to-roll encapsulation of metal nanowires between graphene and plastic substrate for high-performance flexible transparent electrodes. Nano Lett 15:4206–4213

[13] Zhang X, Yan X, Chen J, Zhao J (2014) Large-size graphene microsheets as a protective layer for transparent conductive silver nanowire film heaters. Carbon 69:437–443

[14] Lee D, Lee H, Ahn Y, Jeong Y, Lee D-Y, Lee Y (2013) Highly stable and flexible silver nanowire–graphene hybrid transparent conducting electrodes for emerging optoelectronic devices. Nanoscale 5:7750–7755

[15] Hwang B, Park M, Kim T, Han SM (2016) Effect of RGO deposition on chemical and mechanical reliability of Ag nanowire flexible transparent electrode. RSC Adv 6:67389–67395

[16] Chen D, Liang JJ, Liu C, Saldanha G, Zhao FC, Tong K, Liu J, Pei QB (2015) Thermally stable silver nanowire-polyimide transparent electrode based on atomic layer deposition of zinc oxide on silver nanowires. Adv Funct Mater 25:7512–7520

[17] Hwang B, An Y, Lee H, Lee E, Becker S, Kim Y-H, Kim H (2017) Highly flexible and transparent silver nanowire electrode encapsulated with ultra-thin alumina: thermal, ambient, and mechanical stabilities. Sci Rep 7:41336

[18] Song T-B, Rim YS, Liu F, Bob B, Ye S, Hsieh Y-T, Yang Y (2015) Highly robust silver nanowire network for transparent electrode. ACS Appl Mater Interfaces 7:24601–24607

[19] Vinogradov VV, Agafonov A, Avnir D (2014) Conductive sol–gel films. J Mater Chem C 2:3914–3920

[20] Hwang B, An C-H, Becker S (2017) Highly robust ag nanowire flexible transparent electrode with UV-curable polyurethane-based overcoating layer. Mater Des 129:180–185

[21] Wang J, Jiu J, Sugahara T, Nagao S, Nogi M, Koga H, He P, Suganuma K, Uchida H (2015) Highly reliable silver nanowire transparent electrode employing selectively patterned barrier shaped by self-masked photolithography. ACS Appl Mater Interfaces 7:23297–23304

[22] Jiu J, Wang J, Sugahara T, Nagao S, Nogi M, Koga H, Suganuma K, Hara M, Nakazawa E, Uchida H (2015) The effect of light and humidity on the stability of silver nanowire transparent electrodes. RSC Adv 5:27657–27664

[23] Jin Y, Deng D, Cheng Y, Kong L, Xiao F (2014) Annealing-free and strongly adhesive silver nanowire networks with long-term reliability by introduction of a nonconductive and biocompatible polymer binder. Nanoscale 6:4812–4818

[24] Xu F, Zhu Y (2012) Highly conductive and stretchable silver nanowire conductors. Adv Mater 24:5117–5122

[25] Zeng XY, Zhang QK, Yu RM, Lu CZ (2010) A new transparent conductor: silver nanowire film buried at the surface of a transparent polymer. Adv Mater 22:4484–4488

[26] Moreno I, Navascues N, Arruebo M, Irusta S, Santamaria J (2013) Facile preparation of transparent and conductive polymer films based on silver nanowire/polycarbonate nanocomposites. Nanotechnology 24:275603

[27] Gu H, Tadakamalla S, Huang Y, Colorado HA, Luo Z, Haldolaarachchige N, Young DP, Wei S, Guo Z (2012) Polyaniline stabilized magnetite nanoparticle reinforced epoxy nanocomposites. ACS Appl Mater Interfaces 4:5613–5624

[28] Zhao Y, Barrera EV (2010) Asymmmetric diamino functionalization of nanotubes assisted by BOC protection and their epoxy nanocomposites. Adv Funct Mater 20:3039–3044

[29] Ellis B (1993) Chemistry and technology of epoxy resins. Springer, Berlin

[30] Yim MJ, Paik KW (2006) Review of electrically conductive adhesive technologies for electronic packaging. Electron Mater Lett 2:183–194

[31] Lux F (1993) Models proposed to explain the electrical-conductivity of mixtures made of conductive and insulating materials. J Mater Sci 28:285–301. https://doi.org/10.1007/BF00357799

[32] Zhang Y, Guo J, Xu D, Sun Y, Yan F (2017) One-pot synthesis and purification of ultralong silver nanowires for flexible transparent conductive electrodes. ACS Appl Mater Interfaces 9:25465–25473

[33] Hu H, Liu GJ, Wang J (2016) Clear and durable epoxy coatings that exhibit dynamic omniphobicity. Adv Mater Interfaces 3:1600001

[34] Xu F, Xu W, Mao B, Shen W, Yu Y, Tan R, Song W (2018) Preparation and cold welding of silver nanowire based transparent electrodes with optical transmittances > 90% and sheet resistances < 10 ohm/sq. J Colloid Interface Sci 512:208–218

[35] Zhu S, Gao Y, Hu B, Li J, Su J, Fan Z, Zhou J (2013) Transferable self-welding silver nanowire network as high performance transparent flexible electrode. Nanotechnology 24:335202

[36] Koczkur KM, Mourdikoudis S, Polavarapu L, Skrabalak SE (2015) Polyvinylpyrrolidone (PVP) in nanoparticle synthesis. Dalton Trans 44:17883–17905

[37] Rawat A, Mahavar H, Tanwar A, Singh P (2014) Study of electrical properties of polyvinylpyrrolidone/polyacrylamide blend thin films. Bull Mater Sci 37:273–279

[38] Ge Y, Duan X, Zhang M, Mei L, Hu J, Hu W, Duan X (2017) Direct room temperature welding and chemical protection of silver nanowire thin films for high performance transparent conductors. J Am Chem Soc 140:193–199

[39] Nam S, Song M, Kim DH, Cho B, Lee HM, Kwon JD, Park SG, Nam KS, Jeong Y, Kwon SH, Park YC, Jin SH, Kang JW, Jo S, Kim CS (2014) Ultrasmooth, extremely deformable and shape recoverable ag nanowire embedded transparent electrode. Sci Rep 4:4788

[40] Poire E, Klembergsapieha J, Martinu L, Wertheimer MR, Liang S, Barton SS, Macdonald JA (1993) Modification of active-carbon by hydrophobic plasma polymers. Abstr Pap Am Chem Soc 205:151–163

[41] Gupta B, Plummer C, Bisson I, Frey P, Hilborn J (2002) Plasma-induced graft polymerization of acrylic acid onto poly(ethylene terephthalate) films: characterization and human smooth muscle cell growth on grafted films. Biomaterials 23:863–871

[42] Takke V, Behary N, Perwuelz A, Campagne C (2009) Studies on the atmospheric air-plasma treatment of PET (polyethylene terephthalate) woven fabrics: effect of process parameters and of aging. J Appl Polym Sci 114:348–357

[43] Stokes DJ (2008) Principles and practice of variable pressure environmental scanning electron microscopy. Wiley, Chichester

[44] Skriver HL, Rosengaard N (1992) Surface energy and work function of elemental metals. Phys Rev B 46:7157

[45] Abbott JR, Higgins BG (1988) Surface tension of a curing epoxy. J Polym Sci, Part A-1: Polym Chem 26:1985–1988

[46] Atkins P (1998) Physical chemistry, 6th edn. Freeman, New York

[47] Simmons JG (1963) Electric tunnel effect between dissimilar electrodes separated by a thin insulating film. J Appl Phys 34:2581–2590

[48] Scheideler WJ, Smith J, Deckman I, Chung S, Arias AC, Subramanian V (2016) A robust, gravure-printed, silver nanowire/metal oxide hybrid electrode for high-throughput patterned transparent conductors. J Mater Chem C 4:3248–3255

[49] Göbelt M, Keding R, Schmitt SW, Hoffmann B, Jäckle S, Latzel M, Radmilović VV, Radmilović VR, Spiecker E, Christiansen S (2015) Encapsulation of silver nanowire networks by atomic layer deposition for indium-free transparent electrodes. Nano Energy 16:196–206

[50] Park J-S, Chae H, Chung HK, Lee SI (2011) Thin film encapsulation for flexible am-oled: a review. Semicond Sci Technol 26:034001

[51] El Gouri M, El Bachiri A, Hegazi SE, Rafik M, El Harfi A (2009) Thermal degradation of a reactive flame retardant based on cyclotriphosphazene and its blend with DGEBA epoxy resin. Polym Degrad Stab 94:2101–2106

[52] Celle C, Mayousse C, Moreau E, Basti H, Carella A, Simonato J-P (2012) Highly flexible transparent film heaters based on random networks of silver nanowires. Nano Res 5:427–433

[53] Cui Z, Lü C, Yang B, Shen J, Su X, Yang H (2001) The research on syntheses and properties of novel epoxy/polymercaptan curing optical resins with high refractive indices. Polymer 42:10095–10100

[54] Elechiguerra JL, Larios-Lopez L, Liu C, Garcia-Gutierrez D, Camacho-Bragado A, Yacaman MJ (2005) Corrosion at the nanoscale: the case of silver nanowires and nanoparticles. Chem Mater 17:6042–6052